AIAA-97-0053

Heat-Transfer and Freestream Turbulence Measurements for Improvement of the Ice Accretion Physical Model

M.B. Bragg, S. Lee and C.M. Henze
University of Illinois at Urbana-Champaign
Urbana, IL

35th Aerospace Sciences Meeting & Exhibit
January 6-10, 1997 / Reno, NV

HEAT-TRANSFER AND FREESTREAM TURBULENCE MEASUREMENTS FOR IMPROVEMENT OF THE ICE ACCRETION PHYSICAL MODEL

M. B. Bragg*, S. Lee+ and C. M. Henze+
University of Illinois at Urbana-Champaign

ABSTRACT

Convective heat-transfer measurements were taken on a NACA 0012 airfoil with leading-edge distributed roughness simulating ice-accretion roughness. Roughness heights of 0.35 and 0.75 mm were used and tests were conducted at three tunnel turbulence levels and three Reynolds numbers. Convective heat-transfer coefficients approached three times the clean airfoil values over the roughness at a Reynolds number of 2.25×10^6. Results with tunnel turbulence values as high as 0.95% had little effect on the convective heat transfer prior to boundary-layer transition. Downstream of the roughness the heat transfer was in general less than the predicted turbulent value. A method for measuring the turbulence level in an icing tunnel spray cloud with a conventional hot wire is presented. Preliminary results from the NASA Icing Research Tunnel showed that the elevated turbulence levels with the spray cloud on are due to the nozzle air pressure and the presence of the water has only a small effect.

NOMENCLATURE

h	Heat-transfer coefficient
h_{lam}	Laminar heat-transfer coefficient
h_p	Perturbed heat-transfer coefficient
h_{turb}	Turbulent heat-transfer coefficient
h_u	Unperturbed heat-transfer coefficient
k	Thermal conductivity of air
k/δ	roughness height/boundary-layer thickness
LWC	Liquid water content
MVD	Median volumetric diameter
Pr	Prandtl number
Q_{cond}	Conductive heat flux
Q_{conv}	Convective heat flux
Q_{in}	Heat flux in from the lamps
Q_{rad}	Radiative heat flux
T_{aw}	Adiabatic wall temperature
T_s	Surface temperature
T_{su}	Unperturbed surface temperature
T_{sp}	Perturbed surface temperature
T'	Fluctuation temperature
U	Freestream velocity
U_e	Boundary-layer edge velocity
u', v'	Fluctuation velocity
u'_{rms}	Root mean square of velocity fluctuation
x/c	airfoil coordinate/airfoil chord
δ	Uncertainty of measured values
μ	Viscosity
ρ	Density

INTRODUCTION

Numerous studies have shown that there are two distinct regions of ice formation in the glaze-ice accretion process.[1-4] The smooth region near the stagnation line is characterized by a thin film of water over a uniform layer of ice. This region suddenly changes further downstream into a rough zone. The ice buildup is generally greater in this zone, and there is no film of water present. The smooth/rough boundary has also been observed to propagate upstream with time. Shin[4] has made detailed measurements of the size and spacing of the initial ice roughness that forms in the rough zone on a 21-inch chord NACA 0012 airfoil. The roughness height was found to be between 0.28 mm and 0.79 mm with a spacing of 1 to 1.3 diameter.

The increased ice accretion over the rough zone is thought to be the result of greater convective heat transfer due to the presence of roughness. The importance of surface roughness on convective heat transfer was demonstrated by the studies of heat transfer on actual ice accretion shapes. Van Fossen, et

* Professor, Department of Aeronautical and Astronautical Engineering, Associate Fellow AIAA
+ Graduate Research Associate, Dept. of Aeronautical and Astronautical Engineering, member AIAA

al.,[5] and Arimilli and Keshock[6] measured the heat transfer on glaze-ice shapes on a cylinder. The smooth ice shapes had little effect on the heat-transfer rate when compared to that of the clean cylinder calculated by Frössling.[7] Instead, it was only when roughness was added to the ice shape that significant increases in the heat-transfer rates were observed. Thus it became apparent that surface roughness plays a major role in the ice-accretion process.

It was initially thought that the boundary layer transitioned at this smooth/rough boundary, and that the boundary layer in the rough zone was fully turbulent. This would lead to higher heat-transfer rate in the rough zone and explain the absence of a water film in this zone. However, recent studies by Kerho[8] and Bragg, et al.,[9] on a 21-inch chord NACA 0012 airfoil with roughness similar to those observed by Shin[4] suggested that the boundary layer does not suddenly transition at this smooth/rough boundary. Instead, the boundary layer begins the transition process at this location, but the process is not completed until well downstream (on the order of 500 roughness heights). The heat-transfer rates in the transitional boundary layer would be lower than in a fully turbulent boundary layer. Thus, it was thought that the large increase in the local convective heat-transfer rate required for the rough-zone formation was not driven primarily by the boundary-layer transition, but instead by the local effects on the scale of the size of individual roughness elements. However, since it was not known what the heat-transfer rates are in the roughness-induced transitional boundary layer, this could not be stated with certainty.

The purpose of this study was to acquire heat transfer data immediately downstream of the simulated ice roughness to contribute to the understanding of the glaze-ice accretion process. By comparing these to the fully turbulent heat transfer values, and the boundary-layer measurements, the character of the heat transfer can be better understood. The two roughnesses tested were the same as those studied by Kerho[8] and Bragg, et al.,[9] and effectively bounded the sizes of roughness observed by Shin[4] in initial glaze-ice accretions. A test was also conducted to measure the effect of increased freestream turbulence found in icing tunnels using turbulence generating grids that produced 0.5% and 0.95% turbulence intensities. Since icing tunnel turbulence is not well understood, the results of a preliminary study to measure the turbulence level in an icing cloud are reported. A method is presented using a hot-wire probe and a digital filtering technique to remove the effect of water droplet impacts from the data. Initial data acquired in the NASA Icing Research Tunnel (IRT) are presented.

The following sections of this introduction present a more detailed review of the literature in areas relevant to this study.

Effect of Roughness On Heat Transfer

There have been numerous studies on the effects of surface roughness on convective heat transfer. However, the bulk of these have been on the effects of roughness on a turbulent boundary layer, and there have been few studies done on laminar boundary-layer heat transfer with roughness.

Pinson and Wang[10] measured the effects of leading-edge roughness of various sizes and shapes (sandpaper, cylinder in cross flow, and smooth tape) on heat transfer in a flat-plate laminar boundary layer. When the roughness height was below the critical value that caused transition, it had negligible effect on the heat transfer. When the roughness was near the critical height, the heat-transfer rate immediately downstream of the roughness was not affected. Further downstream (on the order of 300 roughness heights) the heat transfer took on transitional values. However, this was significantly upstream of the location where the natural transition process began. The transitional values lasted until the boundary layer became fully turbulent near the same location as that of the undisturbed case. When the roughness height was 2 or 3 times greater than the critical value, the heat-transfer rate immediately behind the roughness was roughly 30 percent greater than that of a smooth-wall turbulent boundary layer. Further downstream (on the order of 50 roughness heights), the heat-transfer values returned to that of a smooth turbulent boundary layer.

Henry, et. al.[11] studied the effect of large isolated hemispherical roughness elements (with roughness height to boundary-layer thickness k/δ on the order of 1) on heat transfer on a flat plate with a laminar boundary layer and zero pressure gradient. These roughness elements were representative of those found in initial glaze-ice accretions. Increased heat-transfer rates of up to 8 times the laminar values were observed over the roughness elements. However, in the near-wake regions, the heat-transfer rates were only twice that of the undisturbed flat plate. Henry et al.,[11] also observed that the heat-transfer enhancement over the roughness increased with increasing roughness size and Reynolds number.

Poinsatte[12] studied the effects of 1 mm high hemispherical roughness on the leading edge of a 21-inch chord NACA 0012 airfoil. Although the size of the roughness was similar to that observed by Shin,[4] the spacing between the roughness was 7 times greater. He found heat-transfer increase of up to 300% on and

immediately downstream of the roughness, but the roughness was not observed to transition the flow in most cases.

The studies described above provided useful information on the effect of roughness on heat-transfer rates in a laminar boundary layer. However, the location, size, and shape of the roughness used in these studies were not representative of that observed under actual glaze-ice accretion. Also, no previous study compared heat-transfer measurements to detailed boundary-layer measurements such as those available in Kerho[8] and Bragg, et al.[9]

Effect of Freestream Turbulence on Heat Transfer

A major problem encountered in the formulation of an accurate ice-accretion model is that the model is based on the results obtained in icing tunnels which may not accurately reproduce the conditions found in flight through icing clouds. Poinsatte[12] showed that the turbulence intensity in flight through smooth air was less than 0.1%. He also measured the turbulence intensity level of the IRT to be between 0.5 and 0.7% with the spray nozzles turned off. Thus, any results that are obtained in the icing tunnels have to be correlated to actual flight conditions which have lower turbulence levels. In order to do this, the effects of freestream turbulence on convective heat transfer (an important input to the ice accretion process) must be known.

There have been numerous studies that investigated the effects of free-stream turbulence on convective heat transfer. One obvious way that it effects heat transfer is by inducing early boundary-layer transition.[13,14] The free-stream turbulence can also affect the heat-transfer rate in the laminar boundary layer even before it transitions. The effects, however, are different for flows with and without pressure gradients. Several studies have shown that freestream turbulence has no affect on the laminar heat-transfer rate on a flat plate with zero pressure gradient.[15-18] The free-stream turbulence does have an effect on heat transfer in a flow under a favorable pressure gradient, but it was shown to be rather modest. Kestin, et al.,[16] and Junkhan and Serovy[17] reported that below a turbulence intensity of 2%, they found an increase in the laminar heat-transfer rate of less than 10%. Poinsatte[12] reported that the heat-transfer rate on a NACA 0012 airfoil in the IRT was at most 10% higher than that measured in flight. Thus, it appeared that as long as the freestream turbulence is modest (under 2%), it should not significantly affect the heat-transfer rates in a laminar boundary layer.

Measurement of Freestream Turbulence

Turbulence measurements in air are usually made using a hot-wire sensor. Operating thermal anemometers in an icing tunnel or atmospheric cloud droplet conditions, however, requires that a method be developed for separating the droplet strikes from the turbulent fluctuations in the freestream. Several researchers have addressed this problem, and more generally the problem of phase discrimination in any two phase flow.

The use of hot-films and wires for measuring turbulence in rain storms was addressed by Merceret.[19,20] By dropping rain drop size water droplets, 0.3 - 0.5 cm, on hot-wires and hot-films in a plexiglass tube with no flow present, the signal returned when a droplet hit the anemometer sensor was examined. A high spike in the signal was observed that indicated a droplet strike, and noted it was noted that Goldschmidt and Householder[21] had observed a similar spike in work with aerosol droplets. These data were compared to data taken in rain storms with winds less than 20 meters per second from a tower on top of the laboratory. Merceret observed a clearly distinguishable droplet strike signal from a wedge shaped hot-film, but found that hot-wires were not useable in these conditions because the signal from large and small droplets could not be clearly differentiated from the turbulence signal. Goldschmidt, and Householder however, found hot-wire sensors suitable for use as particle concentration and size samplers as well as turbulence sensors.[22]

Hetsroni, Cutler, and Sokolov[23] experimented with the use of hot-wires in particle contaminated flow and described the method used to analyze their data. A threshold voltage was set such that any voltage above it was considered to represent a droplet strike, and "clipper and pickoff" circuits where employed. The "pickoff" circuit passed only signals above the voltage threshold. These were then fed to instruments that counted the number of droplets impinging during a set period of time. The "clipper" circuit passed all voltages below the threshold to dc and true rms voltmeters for measuring time-averaged velocity and turbulence intensity. Because of the remaining "stumps" of the droplet strikes, corrections had to be made to these measurements.

Hetsroni and Sokolov[24] made some important observations when this method was applied to two-phase turbulent jet flow. Droplets 13 microns in diameter were injected into the flow prior to exiting a 25 mm diameter nozzle. The exit velocity was 50 m/sec. Measurements of time-averaged and fluctuating velocities along with droplet flux were taken at several locations downstream of the nozzle. The droplets were

almost immediately swept off the wire and the signal returned quickly to the initial heat transfer level. In filtering the data it was assumed that the signals due to droplet strikes where much higher than those due to turbulent fluctuations. Some small droplets, however, were found to generate signals which were only slightly greater than the turbulent signals and thus fell under the threshold voltage.

Much of the more recent work concerning the use of thermal anemometry in two-phase flow has involved "bubbly flows" of gas bubbles in a liquid flow. While this is a considerably different application, many of the phase discrimination techniques used are applicable in air flows containing water droplets. The relatively large size and slow speed of the bubbles in these flows, allows for careful analysis of the low heat transfer region indicative of a bubble passing the sensor. Such analyses, in which the different regions of the bubble and even the approach of the bubble were detected, were outlined in detail in Bruun,[25] Liu and Bankoff[26] and Farrar, et al.[27] These analyses applied threshold criteria not only to the voltage signal, but also to the slope or first derivative of the signal. Farrar, et al. observed difficulty in detecting partial bubble strikes and small bubbles using a voltage threshold method similar to the observations by Hetsroni and Sokolov.[24] The application of a slope threshold, however, made possible the detection of most of these difficult to detect impingements.

A slope threshold was applied to air flow containing liquid droplets by Ritsch and Davidson.[28] In this work, hot-film measurements where taken in 0.6 m/s duct flow containing 2mm atomized oleic acid particles. The average slope between data points was calculated, and when the slope between any two points exceeded 6 times the average, those points where considered to be in the liquid phase. When the time between particle impingements was large compared to the duration of the event itself, the signals within the spike were replaced by the last value prior to exceeding the slope threshold. It was noted, however, that it was better in cases where the spikes compose a larger portion of the data set to remove the particle spikes and reduce the number of data points. It was also noted that a high data rate, 20 kHz was used by Ritsch and Davidson,[28] was necessary to detect the rapid phase changes.

These studies suggest that thermal anemometry can be used as a practical means of measuring turbulent fluctuations in atmospheric and icing tunnel cloud conditions provided an effective method is used to discriminate the water droplet strikes from the freestream turbulent fluctuations. It is apparent that applying only an amplitude threshold to the digitized signal would likely not be sufficient in detecting small droplets or partial droplet strikes. The detection of a majority of these lower amplitude signals can be accomplished by applying a threshold filter to the slope of the signal.

HEAT-TRANSFER MEASUREMENTS

Experimental Method

The primary purpose of this experiment was to provide heat-transfer data to complement the hot-wire boundary-layer measurements by Kerho[8] and later by Bragg, et al.[9] Thus the test matrix included the cases tested in both of the experiments mentioned above and is shown in Table 1. Measurements were taken at Reynolds numbers of 0.75×10^6, 1.25×10^6, and 2.25×10^6 and with the freestream turbulence levels of 0.1%, 0.5%, and 0.95%. The flow blockage due to the presence of the turbulence grids prevented Re = 2.25×10^6 from being attained. Thus, Re = 2.25×10^6 could not be tested with the turbulence grids.

The model used was the same NACA 0012 model used by Kerho[8] and Bragg, et al.[9] The model had a 21-inch chord and 33.7-inch span, allowing it to span the test section height when it was mounted vertically. It was constructed of foam core which was covered by a fiberglass skin. The surface originally had a glossy-black finish which was wet sanded down to give it a flat-black surface. Because of the flat-black appearance, the model's emissivity was assumed to be 1.

Table 1: Heat-transfer measurement test matrix

	Re		
	0.75×10^6	1.25×10^6	2.25×10^6
0.1% Freestream Turbulence			
Clean Model	X	X	X
0.35mm Roughness	X	X	X
0.75mm Roughness	X	X	X
0.5% Freestream Turbulence			
Clean Model	X	X	
0.35mm Roughness	X	X	
0.75mm Roughness	X	X	
0.95% Freestream Turbulence			
Clean Model	X	X	
0.35mm Roughness	X	X	
0.75mm Roughness	X	X	

The roughness patterns tested in this experiment were identical to those used by Kerho[8] and Bragg, et al.,[9] and were idealized simulations of those observed by Shin[4] in initial glaze-ice accretion. Two types of roughness were tested in this experiment, one with 0.35mm height and another with 0.75 mm height. The roughness had a center to center spacing of 1.3 diameter. Both of the roughnesses were attached spanwise to the model with the leading edge of the roughness 7 mm surface length from the leading edge of the model (which corresponded to x/c = 0.005) and were 0.25-inch wide in chordwise extent.

The schematic of the setup is shown in Fig. 1. The surface temperature of the model was obtained using an Inframetrics model 600 infrared camera on loan from NASA Lewis Research Center. The model was heated using commercially available 250W infrared heat lamps through glass windows. The camera was mounted flush to the wall on a viewing port which was simply a hole that had the same diameter as the camera lens. The model's angle of attack was adjusted until a lift coefficient of less than |±0.001| was obtained. Eight heat lamps were used to heat the model through four windows built into the side wall. The model was heated evenly so that at zero tunnel velocity, the surface temperature varied by less than 1 °F in the spanwise direction and 2 °F in the chordwise direction from x/c = 0.05 to x/c = 0.5. Outside of this range, there was a greater temperature variation. With the model on the test section centerline, the camera's limited field of view allowed only 35% of the chord length to be viewed at once. Thus, four viewing ports were used to obtain the heat-transfer data for the entire chord length.

Figure 2 shows the side view of the NACA 0012 with the heat-transfer measurement regions. The large shaded area was the camera's field of view from viewing port 1. A dark blue masking tape with reflective vertical markings (placed every 10% chord) was used to show the chordwise location in the camera image. The reflective nature of the marking led to a low emissivity, and the markings were very distinctive in the IR images. The roughness tape spanned only half of the camera's field of view. This resulted in both the perturbed (or area downstream of the roughness) and the unperturbed (or area not affected by the roughness) regions of the model being in the IR image.

Figure 3 shows the schematic of the setup for the close up heat-transfer measurements in the vicinity of the roughness. The model was moved so that it was 10 inches from the wall where the camera was mounted. The model was heated by four IR lamps, and the camera was angled so that it would be normal to the model surface at x/c = 0.05.

To generate the 0.5% and 0.95% freestream turbulence levels, biplanar square mesh turbulence generating screens were placed in the test section 30 inches upstream of the leading edge of the model in the same manner as that of Bragg, et al.[9]

Heat-Transfer Calculation

Figure 4 shows the heat transfer on the surface of the model that was heated by the heat lamps. At steady state, an energy balance yields

$$Q_{in} = Q_{conv} + Q_{rad} + Q_{cond} \tag{1}$$

Because the model was constructed of foam and fiberglass which had a very low conductivity, the heat lost through conduction was considered to be very small compared to convective heat loss. Also, radiative heat loss is negligible in wind tunnel experiments performed at low temperatures.[11] Thus, only convective heat losses were considered. Convective heat flux from a surface is given by

$$Q_{conv} = h\left(T_s - T_{aw}\right) \tag{2}$$

Because the heat is assumed to be lost only through convection, at steady state, Q_{in} (from the lamps) should equal Q_{conv}. The convective heat-transfer coefficient can then be written as,

$$h = \frac{Q_{in}}{\left(T_s - T_{aw}\right)} \tag{3}$$

There was no direct way to determine the heat-transfer coefficient because neither Q_{in} nor Q_{conv} was known. Thus a method similar to that of Henry, et al.,[11] was used to calculate the convective heat-transfer enhancement due to the roughness near the leading edge. Since the spanwise heating was assumed to be uniform over the model, the heat-transfer coefficient in the perturbed area of the flow, h_p, downstream of the roughness tape can be normalized by the heat-transfer coefficient in the unperturbed region of the flow, h_u, (i.e. the region of the model not affected by the roughness, but at the same x/c location) by the following equation:

$$\frac{h_p}{h_u} = \frac{\left(T_{su} - T_{aw}\right)}{\left(T_{sp} - T_{aw}\right)} \tag{4}$$

The ratio above will be referred to as the heat-transfer enhancement ratio. In this ratio, $(T_{su}-T_{aw})$ was obtained

from the same run that $(T_{sp}-T_{aw})$ was measured since both perturbed and unperturbed measurements were taken in each run.

Heat-Transfer Measurement Uncertainties

The uncertainty in (T_s-T_{aw}) can be expressed by

$$\delta(T_s - T_{aw}) = \sqrt{(\delta T_s)^2 + (\delta T_{aw})^2} \qquad (5)$$

The uncertainty in the surface temperature measured by the camera was ±1.8 °F at all temperature span settings, and the uncertainty of the adiabatic wall temperature was ±0.5 °F. Therefore, the uncertainty of (T_s-T_{aw}) was ±1.87 °F.

The uncertainty of the heat-transfer ratio (equation (4)) can be expressed by

$$\delta\left(\frac{h_p}{h_u}\right) = \left[\left(\frac{1}{T_{sp}-T_{aw}}\delta T_{su}\right)^2 + \left(\left(-\frac{1}{T_{sp}-T_{aw}} + \frac{T_{su}-T_{aw}}{(T_{sp}-T_{aw})^2}\right)\delta T_{aw}\right)^2 + \left(-\frac{T_{su}-T_{aw}}{(T_{sp}-T_{aw})^2}\delta T_{sp}\right)^2\right]^{1/2} \qquad (6)$$

For a typical case where $(T_{su}-T_{aw})$ was 10 °F and $(T_{sp}-T_{aw})$ was 6 °F, the uncertainty in the heat-transfer ratio was approximately ±35%.

Results and Discussion

The results of this experiment will be presented and discussed in this section. When appropriate, comparisons will be made to the hot-wire results of Kerho[8] and Bragg, et al.,[9] which are summarized in Fig. 5.

Clean Model

The heat-transfer measurements on the clean model without the leading-edge roughness are presented in this section. The measurements were taken without and with the two turbulence-generating grids that produced 0.5% and 0.95% freestream turbulence intensity levels. The heat-transfer measurements are presented as (T_s-T_{aw}) profiles. Since (T_s-T_{aw}) equals Q_{in}/h, and Q_{in} was assumed to be nearly uniform in chordwise extent, (T_s-T_{aw}) can be viewed as an inverse of the heat-transfer coefficient. Also presented are the heat-transfer ratio profiles (h_{Grid}/h_{NoGrid}). These are simply the ratios of the heat-transfer coefficients with and without the turbulence grids at the same x/c location and were determined by dividing (T_s-T_{aw}) without the turbulence grid by (T_s-T_{aw}) with the turbulence grid (in the same manner (h_p/h_u) was calculated).

The clean model temperature and heat-transfer ratio profiles on the NACA 0012 model at Re = $1.25\text{x}10^6$ are shown in Fig. 6. At 0.1% tunnel turbulence, the surface temperature difference increased gradually from the leading edge to x/c = 0.52 as the laminar heat-transfer coefficient decreased with the decreasing wall shear. Between x/c = 0.52 and x/c = 0.70, the temperature decreased due to boundary-layer transition. The temperature started to level off at x/c = 0.70 as the boundary layer became fully turbulent. The temperature profiles at 0.5% and 0.95% tunnel turbulence levels were similar to that of the 0.1% case except for the location of negative temperature gradient where transition occurred. At 0.5% tunnel turbulence, the transition occurred between x/c = 0.35 and x/c = 0.60. At 0.95% tunnel turbulence, the transition occurred between x/c = 0.20 and x/c = 0.60. This was also shown in the heat-transfer ratio profiles.

The $(h_{Grid}/h_{No\ Grid})$ profiles with the 0.5% and 0.95% grids were observed to deviate from 1.0 at x/c = 0.35 and x/c = 0.2, respectively. The results showed that elevated tunnel turbulence (in the range tested) had no significant effect on the heat transfer upstream of the transition location. This was consistent with the results of Kestin, et al.,[16] Junkhan and Serovy,[17] and Poinsatte[12] which showed that freestream turbulence of 1% increased convective heat-transfer rates by less than 10%. It was also interesting that although the transition process at 0.95% tunnel turbulence started significantly upstream of that at 0.5% turbulence, it ended at nearly identical chordwise locations. This resulted in a transition process that was more gradual as the tunnel turbulence level was increased as was shown by the smaller temperature gradient during transition.

Figure 6 also showed that the heat-transfer rates in the turbulent regions with the turbulence grids were lower than that without the grid. This contradicted Junkhan and Serovy[17] who found elevated freestream turbulence intensity having no effect on turbulent heat-transfer rates. One explanation for this difference was the heat lamps that heated the trailing-edge section of the models may have inadvertently moved between runs. This was possible since less care was given to the lighting in the trailing-edge section because the data in this region were deemed not as important as those on other parts of the model.

The heat transfer measurements agreed well with the boundary-layer measurement of Kerho[8] and Bragg,

et al.[9] Figure 7 shows the intermittency contours with varying tunnel turbulence levels at Re = $1.25\text{x}10^6$. At 0.1% tunnel turbulence, Figs. 5 and 7 show that the boundary layer transitioned between x/c = 0.57 and x/c = 0.68 after which it became fully turbulent. This agreed quite well with the heat-transfer measurements and showed that heating the model had no significant effect on boundary-layer development.

At 0.5% tunnel turbulence, Fig. 7 showed elevated boundary-layer intermittency extending downstream from the leading edge. However, near the surface of the model, the intermittency remained low between the leading edge and x/c = 0.35. Downstream of x/c = 0.35, the intermittency was elevated near the surface. Figure 7 also shows that the intermittency near the surface increased from x/c = 0.35 to x/c = 0.55 where it became 1, indicating that a fully turbulent flow had developed near the wall. This corresponded to the region of negative temperature gradient in Fig. 6. Figure 7 shows that the elevated boundary-layer intermittency started at the leading edge for the 0.95% tunnel turbulence level case. However, as in the 0.5% turbulence case, the intermittency near the surface remained low until x/c = 0.20. The intermittency near the surface grew gradually between x/c = 0.2 and x/c = 0.46, where it became 1. This again corresponded to the region of negative temperature gradient in Fig. 6. Thus, although the boundary layer under elevated freestream turbulence appeared transitional from the leading edge, the heat-transfer rates were not affected until the turbulence intensity and intermittency became elevated near the surface. This was expected since surface convective heat-transfer rates are largely dependent on the turbulence quantities $\overline{T'v'}$ and $\overline{u'v'}$ near the surface.[29] Elevated intermittency shown on Fig. 7 was a good indication of elevated $\overline{u'^2}$, $\overline{T'v'}$ and $\overline{u'v'}$. Also, the increase in the surface intermittency was more gradual in the 0.95% turbulence grid case than in the 0.5% case. This again agreed with the heat-transfer measurement of Fig. 6 which showed a more gradual transition process as the freestream turbulence intensity was increased from 0.5% to 0.95%.

The heat-transfer measurements on the clean model at Re = $0.75\text{x}10^6$ and $2.25\text{x}10^6$ showed trends that were similar to those shown above at Re = $1.25\text{x}10^6$. The results also compared very well to those of Kerho[8] and Bragg, et al.[9]

Heat-Transfer Enhancement due to Roughness

In the following section, the heat-transfer enhancement effects due to large leading-edge roughness are discussed. The data presented were taken without the presence of the turbulence generating grids so the freestream turbulence intensity levels were less than 0.1%. The heat-transfer increase is presented as the ratio (h_r/h_u) of the heat-transfer coefficient in the region perturbed (or affected) by the roughness to the heat-transfer coefficient of the unperturbed laminar boundary layer at the same x/c location.

The heat-transfer ratios were also compared to the analytically calculated heat-transfer ratio (h_{turb}/h_{lam}). The laminar heat-transfer coefficients were obtained using the STAN5[30] heat-transfer code. Although it worked well for a laminar boundary layer, the STAN5 code did not provide satisfactory turbulent heat-transfer coefficient in a favorable pressure gradient. Thus, the turbulent heat-transfer coefficients were obtained from the solution of the energy-integral equation developed by Ambrok[31]. Here, the turbulent heat-transfer coefficient is given by,

$$h_{turb} \approx 0.0295 \frac{k\rho^{0.8} U_e \, Pr^{0.6}}{\mu^{0.8} \left[\int_0^x U_e \, dx \right]^{0.2}} \qquad (7)$$

Figure 8 shows the heat-transfer ratio (h_r/h_u) with the 0.35mm roughness at Re = $0.75\text{x}10^6$, $1.25\text{x}10^6$, and $2.25\text{x}10^6$. The heat-transfer ratio was approximately 1 from the leading edge to x/c = 0.007. At Re = $0.75\text{x}10^6$, the heat-transfer ratio rose from 1 to 1.2 between x/c = 0.007 and 0.014. This coincided well with the location of the roughness tape which was between x/c = 0.0050 and x/c = 0.0138. The heat-transfer ratio then decreased until it reached 1 again at x/c = 0.025 and stayed constant. The results showed that the 0.35mm roughness at Re = $0.75\text{x}10^6$ did not significantly alter the heat-transfer characteristics on the model, except on the roughness itself, and in the region immediately downstream. This agreed with the boundary-layer measurements shown in Fig. 5, which showed that the 0.35mm roughness had no effect on the development of the boundary layer.

At Re = $1.25\text{x}10^6$, the heat-transfer ratio profile remained approximately 1 between the leading edge and x/c = 0.007. Between x/c = 0.007 and x/c = 0.017, the heat-transfer ratio was observed to increase sharply from 1 to 1.7 as it became affected by the roughness. It then decreased to 1.5 at x/c = 0.03 after which it began to gradually increase again. Immediately downstream of the roughness, the heat-transfer ratios were higher than those of the theoretical (h_{turb}/h_{lam}) values. Pinson and Wang[10] showed that when the roughness height was 2 or 3 times that of the critical value, the heat-transfer rates immediately downstream of the roughness were elevated beyond that of a smooth wall turbulent

boundary layer. Poinsatte[12] also showed that the heat-transfer rates over and immediately behind the roughness was higher than that of a smooth wall turbulent boundary layer. And finally, Henry, et al.,[11] showed that the heat-transfer enhancement ratio (h_r/h_u) with the roughness of the size studied in this experiment was as high as 8 directly over the element. However, this was the peak value on top of an element, and the measurements shown in this study are averaged heat-transfer values over multiple roughness elements.

Figure 8 shows that the high heat-transfer rate did not extend far in the chordwise direction. In fact, at x/c = 0.10, the heat-transfer rates were on the order of only 75% of that of the theoretical (h_{turb}/h_{lam}) values. This indicated that the boundary layer was not fully turbulent. This was similar to the pre-transitional heat-transfer rates observed by Pinson and Wang[10] on a flat plate with leading-edge roughness near critical height. Again, this compared well with boundary-layer measurements shown in Fig. 5 which showed that the boundary layer behind the roughness was transitional until it became fully turbulent at x/c = 0.5.

At Re = 2.25×10^6, in Fig. 8, there was a sharp increase in the heat-transfer ratio between x/c = 0.005 and x/c = 0.018 due to the roughness. The heat-transfer ratio then decreased to 1.7 at x/c = 0.04 where it started to gradually increase again. As in the Re = 1.25×10^6 case, the heat-transfer ratio immediately downstream of the roughness was greater than that of the theoretical (h_{turb}/h_{lam}) values. However, downstream of x/c = 0.05, (h_r/h_u) was significantly lower than (h_{turb}/h_{lam}) since as Fig. 5 shows, the boundary layer was transitional and not fully turbulent.

From Fig. 8 it is seen that as Reynolds number was increased, (h_r/h_u) increased as well. This followed the theoretical trends and agreed with the results obtained by Henry, et al.[11]

Figure 9 shows the heat-transfer ratio profiles with 0.35mm and 0.75 mm roughness at Re = 1.25×10^6. It shows that the size of the roughness had a negligible effect on the heat-transfer characteristics on the model. Both of the roughnesses initiated the early transition process with the resulting boundary layer far downstream of the roughness having transitional heat-transfer characteristics. The heat-transfer ratio over the roughness did not seem to be affected significantly by the change in the roughness size. The profile with the 0.75 mm roughness had slightly greater values but were well within the uncertainties of the measurement.

Figure 10 shows the heat-transfer ratio profiles with the 0.35 mm roughness at Re = 1.25×10^6. From the leading edge to x/c = 0.20, the elevated freestream turbulence had a negligible effect on the heat-transfer enhancement due to the leading-edge roughness. The results, however showed that at 0.5% and 0.95% tunnel turbulence levels, the heat-transfer ratio profiles began to diverge from that obtained without the turbulence grid at x/c = 0.2 and x/c = 0.35, respectively. This was due to the unperturbed boundary layer undergoing early transition due to increased freestream turbulence as discussed previously. Thus, the results showed that elevated freestream turbulence had little effect on laminar heat-transfer rates.

Boundary-layer measurements by Kerho[8] and Bragg, et al.,[9] showed that the perturbed boundary layer took on increasingly turbulent characteristics as the distance from the roughness was increased. Thus, it was thought that the heat-transfer ratio profiles should approach the theoretical (h_{turb}/h_{lam}) profiles with increasing x/c. However, the heat-transfer ratio profiles shown in Fig. 9 did not approach the theoretical (h_{turb}/h_{lam}) values even as the perturbed boundary layer became fully turbulent while the unperturbed boundary layer remained laminar. It was speculated that there may have been an offset error in the far-field (T_r-T_{aw}) values which resulted in heat-transfer ratios that were too low. Figure 11 shows the result of accounting for the possible offset error. The heat-transfer ratio profiles with 0.75mm roughness at Re = 0.75×10^6 are shown. Shifting the (T_{sp}-T_{aw}) and (T_{su}-T_{aw}) profiles down by 2.2 °F resulted in a heat-transfer ratio that approached the theoretical profile with increasing x/c. Given the experimental uncertainties associated with the infrared spectroscopy method, it was not at all unlikely that there was an offset error of this magnitude. However, the general trend of the shifted and unshifted heat-transfer profiles remained the same. The shifted heat-transfer rate downstream of the roughness was below that of a fully turbulent boundary-layer and did not approach turbulent values until x/c = 0.2. Therefore, regardless of the possible error, the roughness caused increased heat transfer over and just downstream of the roughness, followed by a region where the heat transfer was less than the fully turbulent value.

TURBULENCE MEASUREMENTS IN CLOUDS

The role of freestream turbulence in the ice accretion process is still not completely understood. Measurements reported earlier in this paper suggest that while it changes the boundary-layer development, the heat transfer is affected to a lesser degree. However, ice roughness extends well above the boundary layer and its heat transfer may be affected differently. This effect can not be properly evaluated until the turbulence in an icing cloud on the a scale appropriate to the ice

accretion problem is better understood. Reported below is a method, and some preliminary results from the NASA Icing Research Tunnel, which may provide some insight into this area.

Method Development

Figure 12 shows the trajectories of three different size droplets as they pass above a 21-inch chord NACA 0012 airfoil at eight degrees angle of attack and a freestream velocity of 100 mph. The momentum of these droplets, which just miss impinging on the upper surface of the airfoil, carries them above the surface. As the size of the droplets decreases, this momentum decreases and the droplets pass closer to the airfoil. Due to this effect, the mass of water in the flow in an icing tunnel should be reduced above the trailing edge of an airfoil at angle of attack. By mounting a hot-wire probe in this location, the shielding effect will reduce the influence of the water droplets on the measurement. Thus, if the objective is to obtain the turbulence intensity of the freestream air in this two-phase flow, the amount of water contaminated data which must be removed by filtering can be reduced to allow for an effective turbulence intensity measurement. Allowance for the airfoil boundary layer must be made so as not to contaminate the measurements of the freestream turbulence.

Tests were performed in the UIUC low-speed wind tunnel to examine the effect of the airfoil on the turbulence intensity measurements. The hot-wire sensor was mounted on a strut which entered the test section through a span-wise slot. The strut was attached to a 2-dimensional traverse which was housed in a pressure sealed box adjacent to the test section as shown in Fig. 13. For a more detailed description of this setup see Kerho.[8] The traverse allowed the sensor to be placed above the 21-inch chord NACA 0012 model at approximately the 85% chord station.

Output from an IFA-100 anemometer system was digitized at 10 kHz and recorded using an A/D conversion board in a Pentium PC. The low-pass filter was set at 5 kHz and a 3 Hz high-pass filter was used to remove low-frequency velocity fluctuations. Data sets were taken over a 3-second period to acquire 30,000 samples. Two signal conditioners contained in the IFA-100 system were used. The output of the first signal conditioner was the full dc signal and signal conditioner 2 was used to perform the high-pass filtering. The data were acquired on separate A/D channels to obtain the mean voltage from the DC channel and the fluctuating signal from the second signal conditioner output. The fluctuating signal was also supplied to a Wavetek spectrum analyzer for recording frequency spectrums.

Velocity values were calculated from the voltage readings using calibrations for each wire. All hot-wire data were corrected for temperature and density variations. Turbulence intensity levels, u'_{rms}, were calculated from the velocity values using:

$$u'_{rms}(\%) = \frac{100}{U}\left[\frac{1}{T}\int_0^T (u')^2\, dt\right]^{1/2} \qquad (8)$$

where T is the total time, and U is the mean velocity, and u' is the fluctuation from the mean velocity.

Figure 14 shows the results of some of these tests. Here the tunnel velocity was approximately 100 mph and the probe was placed 1.5 inches from the model surface. The variation of turbulence intensity with angle of attack is shown at low and high turbulence levels in the UIUC tunnel, and in the IRT. In the high turbulence UIUC tunnel case, a grid was installed in the test section upstream of the model to increase the turbulence intensity level to values near those in the NASA Lewis Icing Research Tunnel. At moderate angles of attack, and particularly at the higher turbulence levels, the model angle of attack has very little effect on the turbulence values. Figure 15 is a plot of the turbulence intensity level versus probe distance from the model under the same high turbulence conditions in the UIUC tunnel. With the model at 8 degrees angle of attack, the turbulence intensity measurement varies only slightly until the probe is in the boundary layer at 0.5 inches from the surface. Based on these tests, the effect of the model on the measured freestream turbulence intensity was not significant if the probe was at least one inch above the airfoil surface and the airfoil angle of attack was less than 10 degrees.

During testing in the Icing Research Tunnel at the NASA Lewis Research Center the hot-wire sensor was mounted above a 21-inch NACA 0012 model as shown in Fig. 16. The probe was located at approximately 85% chord, and could be moved from 0.5 to 6 inches from the model surface in 0.5 inch increments. The data acquisition setup was the same as in the UIUC tunnel with the following changes. Data were digitized at 100 kHz to make it possible to resolve the rapid heat transfer changes caused by water droplet impingement on the sensor. The data were high-pass filtered at 0.1 Hz and low-pass filtered at 100 kHz by the IFA-100 system. Data sets of 100,000 samples (1 second duration) were obtained.

It was obvious from initial tests that a considerable number of droplets were still striking the sensor even with the wire 1.5 inches from the model surface, and the model at 10 degrees angle of attack. This was probably due to smaller droplets in the cloud passing close to the model, and/or droplets being swept closer to the model by large-scale turbulent fluctuations. However, the model was providing some shielding of the sensor from the water in the flow. With the probe 1.5 inches from the model surface, the angle of attack of the model was varied from 0 to 8 degrees in a cloud of 30 micron droplets with a liquid water content (LWC) of 1.5 g/m^3. The freestream velocity was approximately 100 mph. The results of this angle of attack sweep are shown in Fig. 17 where the rms of the velocity was calculated using the full data set including the droplet strikes. The significant decrease in rms with increasing angle of attack indicates that the model was indeed shielding the sensor.

The shielding effect of the model was also apparent in ice accretions on the probe support. While most of the IRT tests were performed at temperatures above freezing to avoid ice accretion on the sensor, some tests were done at colder temperatures to ascertain the usefulness of this method in icing conditions. Figure 18 is a photograph of the probe and its mounting support from above (see Fig. 16 for a diagram of the support) with ice accreted on the leading edge of the airfoil shaped support. The model was at 8 degrees angle of attack and the shielding effect of the airfoil can be observed in the decreased ice accretion near the model.

Time traces of velocity and acceleration data are shown in Figs. 19 and 20. These plots are for a freestream velocity of approximately 100 mph in a droplet cloud of median volumetric diameter (MVD) = 30 microns and LWC = 1.5g/m^3. The model angle of attack was set at 8 degrees, and the sensor was 1.5 inches from the model surface. Time traces for the same conditions with no water present are also plotted for comparison. Figure 19 is a 0.01 second time trace of the velocity and acceleration, while Fig. 20 shows 0.002 seconds of the same. The importance of using an acceleration as opposed to a velocity threshold filter, as noted by Farrar et al.[27] in their work in bubbly flows, is apparent here. While the larger spikes due to droplets are clearly apparent in the velocity plots some of the smaller spikes, probably due to small drops or partial droplet strikes are difficult to differentiate from freestream turbulence. Plotting the accelerations makes even the smaller spikes considerably more apparent. The magnitude of the maximum acceleration in the no water case was 80,572.21 ft/s^2, while the maximum acceleration in the water on case was drastically higher at almost 10 million ft/s^2.

The acceleration threshold filtering method used in this study is illustrated in Fig. 21. A threshold, indicated by the two horizontal lines, is set just above the maximum absolute acceleration of a corresponding data set with no spray on. In almost all the cases at 100 mph, 100,000 ft/s^2 was found to be an appropriate threshold level. When an acceleration exceeds this value it was considered to be part of a response to a droplet impingement. All data 0.0001 seconds before and after this event are then marked to be excluded from turbulence intensity calculations. In Fig. 21 the data removed by the filter are indicated by the gray lines. Some small spikes in these data, such as at t = 0.3727 seconds, may be small droplet or partial droplet strikes that fall below the threshold and are not removed by the filter.

The results of applying this filtering are shown in Fig. 22. This plot is for the same conditions as Figs. 19-21. The turbulence intensity level of the filtered data set approaches that of the corresponding water-off case as the filter threshold setting decreases. It appears that some small droplets still circulating in the tunnel caused a few small spikes in the water-off data. This resulted in the high maximum acceleration, 137,000 ft/s^2, noted by the vertical line in Fig. 22. Applying a 100,000 ft/s^2 threshold filter to this water-off data only removed 0.047% of the data and resulted in a drop of 0.001% in turbulence intensity, so a threshold of 100,000ft/s^2 is still appropriate here. The amount of data removed from this particular water-on data set, approximately 77% at a threshold level of 100,000 ft/s^2, was quite large. However, the filtered turbulence intensity levels still fall near the expected water-off value. Applying the filter to data sets where the LWC was lower resulted in far less data being removed. In Figure 23 data are shown for the same conditions as in Fig. 21 except that the LWC was reduced to 0.9 g/m^3. In this case only about 12% of the data were removed by a threshold of 100,000 ft/s^2.

Preliminary IRT Results

The primary purpose of these tests was to evaluate the method for measuring turbulence levels in icing tunnel and cloud conditions. However, some interesting preliminary results were found and will be presented here. Because this was a preliminary test, and due to time constraints in the IRT, only a limited set of data and repeat runs could be made. More data will be required before some of the apparent inconsistencies in these data can be resolved.

The NASA Mod-1 icing spray nozzles used in the IRT produce a jet of fine water droplets when high-

pressure air atomizes a stream of water as it exits the nozzle. The combination of nozzle water and air pressure settings at a given tunnel velocity are used to set the MVD and LWC of the droplet cloud. One objective of these tests was to explore the effects of nozzle air and water pressure on turbulence intensity. It is well known that nozzle air pressure increases the tunnel turbulence level, but the effect of water pressure has been unknown due to a lack of a measurement technique.

To study nozzle air pressure effects, the probe was mounted on its support 6 inches away from the model surface and the model angle of attack was set at zero degrees. This sensor location provided the least possible influence from the model using the current mounting system. The tunnel velocity was set at approximately 100 mph, and data were taken at increasing nozzle air pressures with no water pressure to the nozzles. Figure 24 presents these data. The increase in freestream turbulence level with increasing nozzle air pressure was significant with an increase in turbulence intensity from 0.59% with no air pressure to 0.88% with nozzle air pressure at 80 psi. Poinsatte[12] found turbulence levels of 0.6%, 0.52%, and 0.7% at 70, 140, and 210 miles per hour respectively with no nozzle air pressure. These values compared well to the turbulence level of 0.53% found in the current study with the nozzle air off. Similar increases in turbulence intensity because of nozzle air pressure were found by Gonsalez.[32] The increase in turbulence with air pressure was likely because of the turbulence generated in the stream as the nozzles exhausted air at high velocity and with a significant crossflow component. High velocity jets in crossflow have been shown to produce a turbulent wake and this was likely the effect which increased the IRT turbulence level as nozzle air pressure was increased.

The effect of nozzle water pressure on turbulence level was also explored. The model was set at eight degrees angle of attack and the sensor mounted 1.5 inches from the model surface. With the tunnel at 100 mph, nozzle water pressure was increased from 0 to 100 psi at nozzle air pressures of 20, 30, and 40 psi. The results are shown in Fig. 25. Again, an overall increase in turbulence level with increased nozzle air pressure was seen. Nozzle water had little effect on the turbulence intensity, especially at low water pressures. Unfortunately, all of these data were at relatively high LWCs , and, as noted earlier, large amounts of data were removed. The influence of the water droplets may not have been completely removed due to small spikes which were undetected by the filtering technique. This, along with being limited to only 2 repeat data sets at each condition, could possibly explain the apparent turbulence increase in the 30 psi air pressure case, and the low turbulence point at 40 psi air pressure.

Turbulence data were taken over a range of droplet sizes and water contents in the IRT. These results are presented in Fig. 26. The general trend which emerged was an increase in turbulence intensity as droplet size and liquid water content increased. As indicated by the trends in turbulence with nozzle water and air pressures, this increased turbulence was primarily because of higher nozzle air pressures at higher LWC and MVDs. Water-off cases at the same nozzle air pressures are plotted for comparison. In general, the turbulence intensities calculated after filtering water droplets from the spray-on cases were slightly higher than those from water-off data. This could be a real effect or becuase of inadequate filtering of the droplet impingement on the sensor. The small increase in turbulence intensity measured with the spray-on was probably within the accuaracy of the present filtering technique

As mentioned earlier, some data were taken at freezing temperatures to determine if this method could be used in icing conditions. The data taken soon after the spray nozzles were turned on were successfully filtered and turbulence levels near the no-spray case were obtained. In only a few minutes, however, ice began to accrete on the prongs of the hot-wire sensor, and the data were no longer meaningful. Therefore, this method could be used if the sensor support prongs and structure could be properly anti-iced or periodically de-iced.

CONCUSIONS

The following conclusions can be drawn based on the heat-transfer measurements:

1. The heat transfer on the clean model remained laminar, even with elevated tunnel turbulence, until the transition process began.
2. Increased heat transfer with tunnel turbulence correlated to increased turbulence intermittency at the wall.
3. Heat-transfer rates over and immediately downstream of the roughness were higher than the corresponding turbulent values.
4. Further downstream of the roughness the heat transfer fell below the turbulent values.
5. Increased Reynolds number increased the heat transfer over and just downstream of the roughness.

The preliminary tunnel turbulence measurements in the spray could yielded these conclusions:

1. The effect of the droplet impingement on the hot-wire sensor could be effectively removed.
2. With some modification the method could be used at lower temperatures when ice was accreting.
3. Preliminary IRT results showed a significant increase in tunnel turbulence with nozzle air pressure but little effect of nozzle water pressure.

ACKNOWLEDGMENTS

This research was supported in part by grant NAG3-1681 from NASA Lewis Research Center. The authors wish to thank Dr. Dave Anderson and the staff at the NASA Lewis Icing Research Tunnel for their contributions to this research. The authors also acknowledge Mr. Mario Vargas from NASA for his assistance with the infrared camera and Mr. Jonanthan Reichhold of UIUC for his assistance in acquiring the hot-wire data.

REFERENCES

[1]Hansman, R.J., Yamaguch, K., Berkowitz, B., and Potapczuk, "Modeling of Surface Roughness Effects on Glaze Ice Accretion," AIAA Paper 89-0734, Jan. 1989

[2]Hansman, R.J., Reehorst, A., and Sims, J., "Analysis of Surface Roughness Generation in Aircraft Ice Accretion," AIAA Paper 92-0298, Jan. 1992

[3]Hansman, R.J., "Microphysical Factors Which Influence Ice Accretion," *Proceedings of the First Bombardier International Workshop on Aircraft Icing/Boundary-Layer Stability and Transition*, Sept. 1993

[4]Shin, J., "Characteristics of Surface Roughness Associated with Leading Edge Ice Accretion," AIAA Paper 94-0799, Jan. 1994

[5]Van Fossen, G.J., Simoneau, R.J., Olsen, W.A., and Shaw, R.J., "Heat Transfer Distribution Around Nominal Ice Accretion Shapes Formed on a Cylinder in the NASA Lewis Icing Research Tunnel," NASA TM-83557, 1984

[6]Arimilli, R.V. and Keshock, E.G., "Measurements of Local Convective Heat Transfer Coefficinets on Ice Accretion Shapes," AIAA Paper 84-0018, AIAA 22nd Aerospaces Sciences Meeting, Reno, NV, 1984

[7]Frössling, N., "Evaporation, Heat Transfer, and Velocity Distribution in Two-Dimensional and Rotationally Symmetrical Laminar Boundary-Layer Flow," NACA TM-1432

[8]Kerho, M.F., "Effect of Large Distributed Roughness Near an Airfoil Leading Edge on Boundary-Layer Development and Transition," Ph.D. Dissertation, University of Illinois at Urbana-Champaign, 1995

[9]Bragg, M.B., Cummings, M.J., Lee, S., and Henze, C.M., "Boundary-Layer and Heat-Transfer Measurements on an Airfoil with Simulated Ice Roughness," AIAA Paper 96-0866, 34th Aerospace Sciences Meeting & Exhibit, Reno, NV, 1996

[10]Pinson, M. and Wang, T., "Effects of Leading-Edge Roughness on Fluid Flow and Heat Transfer in the Transitional Boundary Layer Over a Flat Plate," ASME Paper 94GT-326, 1994

[11]Henry, R.C., Hansman, R.J., and Breuer, K.S., "Measuremant of Heat Transfer Variation on Surface Roughness Elements Using Infrared Techniques," Paper AIAA-94-0801, AIAA 32nd Aerospace Sciences Meeting & Exhibit, Reno, NV, Jan. 10-13, 1994,

[12]Poinsatte, P.E., "Heat Transfer Measurements From a NACA 0012 Airfoil in Flight and in the NASA Lewis Icing Research Tunnel," M.S. Thesis, The University of Toledo, Toledo, OH, NASA CR-4278, 1990

[13]Schubauer, G.B. and Skramstad, H., "Laminar Boundary Layer Oscillation and Transition on a Flat Plate," NACA Report 909, 1948

[14]Spangler, J.G. and Wells, C.S., "Effect of Freestream Disturbance on Boundary Layer Transition," *AIAA Journal*, Vol. 6, pp. 534-545

[15]Edwards, A. and Furber, B.N., "The Influences of Free-Stream Turbulence on Heat Transfer by Convection From an Isolated region on a Plane Surface in Parallel Air Flow," *The Institution of Mechanical Engineers Proceedings*, Vol. 170, 156, pp. 941-954

[16]Kestin, J. Maeder, P.F., and Wang, H.E., "Influences of Turbulence on the Transfer of Heat From Plates With and Without a Pressure Gradient," International Developments in Heat Transfer, International Heat Transfer Conference, University of Colorado and

London, England, American Society of Mechanical Engineers, 1961, pp. 432-438

[17]Junkhan, G.H. and Serovy, G.K., "Effects of Free-Stream Turbulence and Pressure Gradient on Flat-Plate Boundary-Layer Velocity Profiles and on Heat Transfer," *ASME Journal of Heat Transfer*, May 1967, pp. 169-175

[18]Wang, T., Simon, T.W., Buddhavarapu, J, "Heat Transfer and Fluid Mechanics Measurements in Transitional Boundary Layer Flows," *ASME Journal of Engineering for Gas Turbines and Power*, Oct. 1985, Vol. 107, pp. 1007-1015

[19]Merceret, F.J., "An Experimental Study to Determine the Utility of Standard Commercial Hot-wire and Coated Wedge-Shaped Hot-film Probes for Measurement of Turbulence in Water-Contaminated Air Flows," Technical Report #40, Chesepeake Bay Institute, The John's Hopkins University, 1968

[20]Merceret, F.J., "An Experimental Study to Determine the Utility of Standard Commercial Hot-wire and Coated Wedge-Shaped Hot-film Probes for Measurement of Turbulence in Water-Contaminated Air Flows, Part II," Technical Report #40, Chesepeake Bay Institute, The John's Hopkins University, 1969

[21]Goldschmidt, V.W. and Householder, M.K., "Turbulent Diffusion and Impaction of Aerosol Droplets on Fine Wires," Informal Annual Report, NSF Grant GK00324, Purdue University, September 1966.

[22]Goldschmidt, V.W. and Householder, M.K., "The Hotwire Anemometer as an Aerosol Droplet Size Sampler," Atmospheric Environment, Pergamon Press, 1969, Vol. 3, pp. 643-651

[23]Hetsroni, G., Cutler, J.M., and Sokolov, "Measurements of Velocity and Droplets Concentration in Two-Phase Flows," Journal of Applied Mechanics, Transactions of the ASME, June 1969, pp. 334-335

[24]Hetsroni, G., and Sokolov, "Distribution of Mass, Velocity, and Intensity of Turbulence in a Two-Phase Turbulent Jet," Journal of Applied Mechanics, Transactions of the ASME, June 1971, pp. 315-327

[25]Bruun, H.H., "Hot-Wire Anemometry: Principles and Signal Analysis," section 9.9.1 and 9.9.2, Oxford University Press, 1995

[26]Liu, T.J., and Bankoff, S.G., "Structure of Air -Water Bubbly Flow in a Vertical Pipe I. Liquid Mean Velocity and Turbulence Measurements," International Journal of Heat and Mass Transfer, Vol. 36, No. 4, pp. 1049-1060

[27]Farrar, B., Samways, A.L., Ali, J., and Bruun, H.H., "A computer-Based Hot-Film Technique for Two-Phase Flow Measurements," Meas. Sci. Technol. 6, 1995, pp. 1528-1537

[28]Ritsch, M.L. and Davidson, J.H., "Phase Discrimination in Gas-Particle Flows Using Thermal Anemometry," Journal of Fluids Engineering, Transactions of the ASME, Vol. 114, December, 1992, pp. 692-694

[29]Cebeci, T. and Bradshaw, P., *Physical and Computational Aspects of Convective Heat Transfer*, Springer-Verlag, New York, 1984

[30]Crawford, M.E. and Kays, W.M., "STAN5 - A Program for Numerical Computation of Two-Dimensional Internal and External Boundary Layer Flows," NASA CR-2742, 1976

[31]Ambrok, G.S., "Approximate Solutions of Equations for the Thermal Boundary Layer with Variations in the Boundary Layer Structure," *Soviet Phys.-Tech. Phys.*, 1957, Vol. 2, No. 9, pp. 1979-1986

[32]Gonsalez, J.C., NASA Lewis Research Center, Cleveland, Ohio, personal communication, June, 1996.

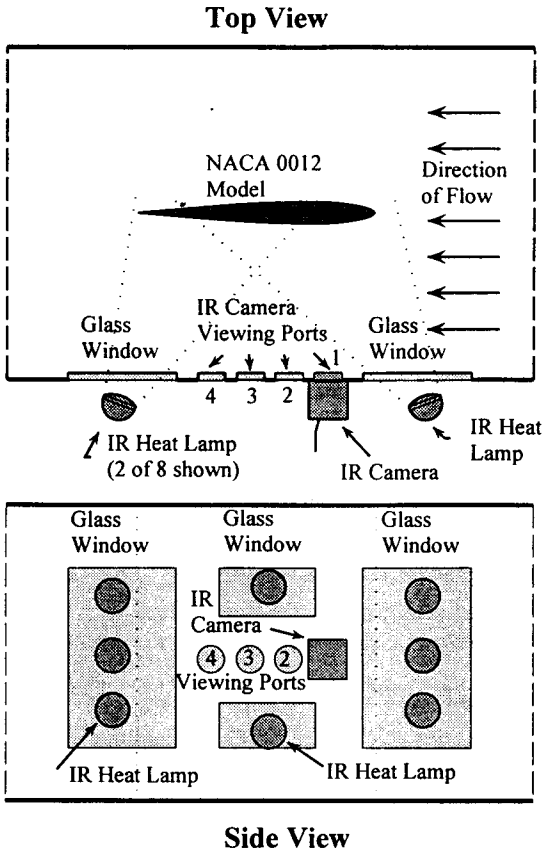

Fig. 1: Schematic of the setup for heat-transfer measurements.

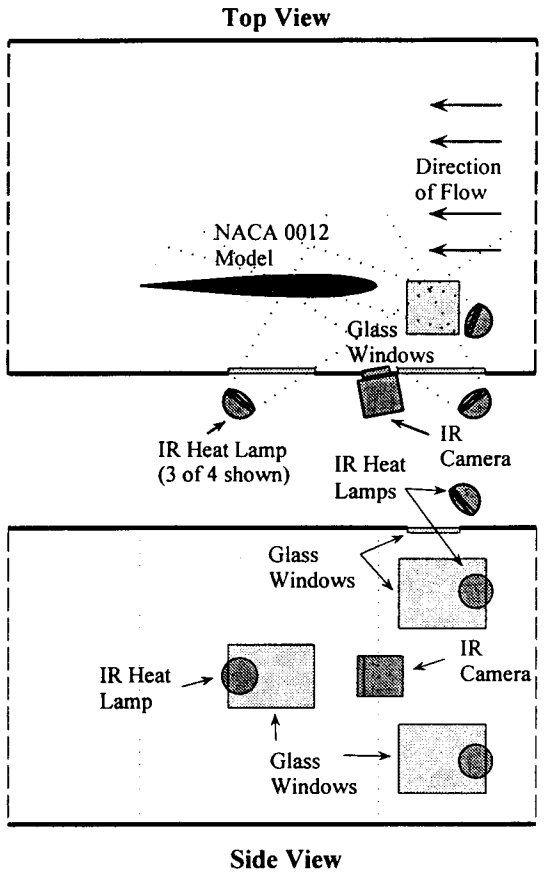

Fig. 3: Schematic of the setup for close-up heat-transfer measurements.

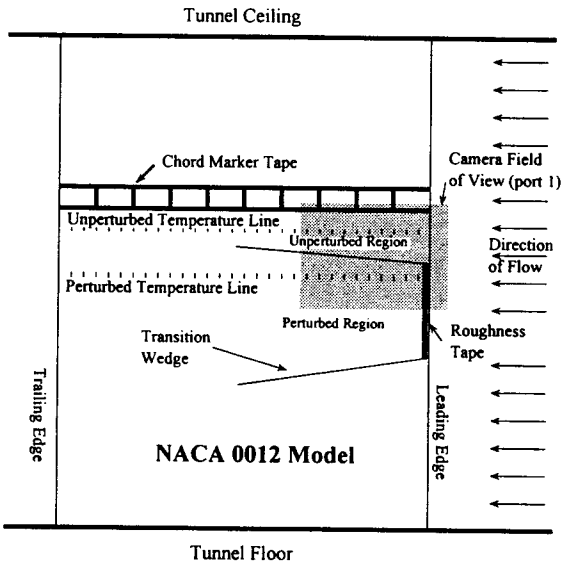

Fig. 2: Side view of the model showing heat-transfer measurement regions.

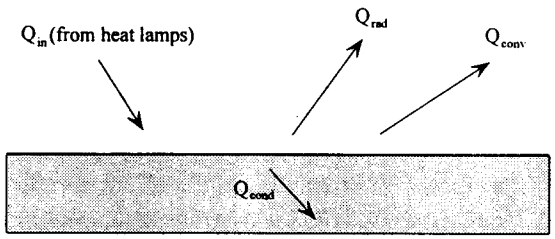

Fig. 4: Modes of energy transfer of a heated surface.

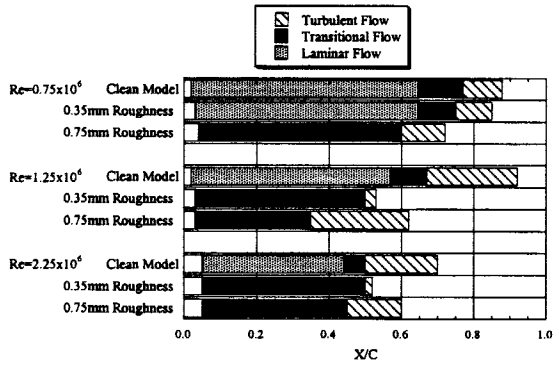

Fig. 5: Boundary-layer state summary of Kerho[8] and Bragg, et al.,[9] categorized by Reynolds number and roughness height.

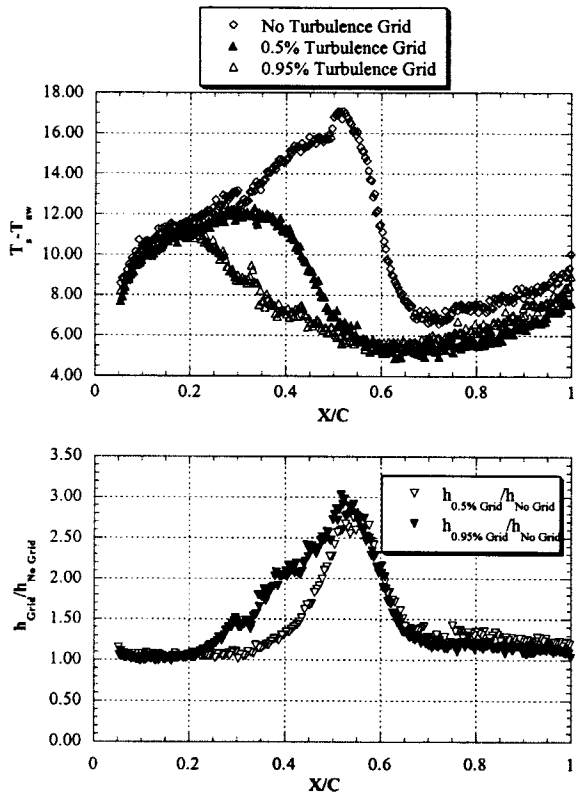

Fig. 6: Surface temperature and heat-transfer ratio profiles on the clean model with varying tunnel turbulence levels. (Re=1.25x10^6)

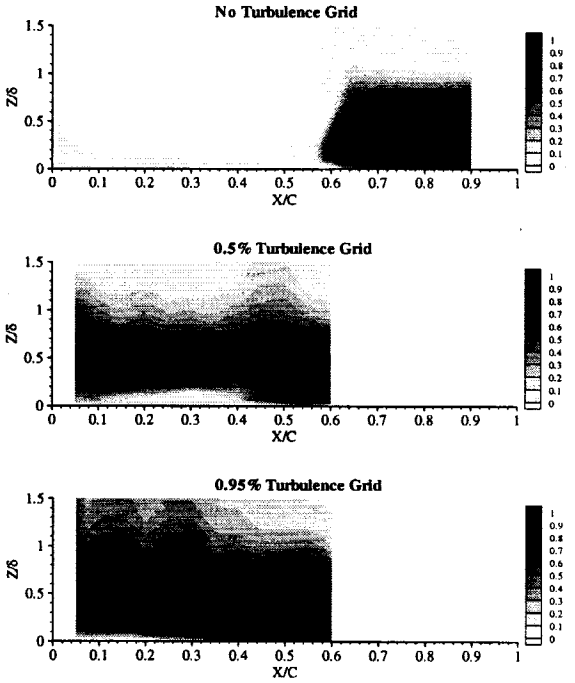

Fig. 7: Clean model intermittency contours with varying tunnel turbulence.[9] (Re=1.25x10^6)

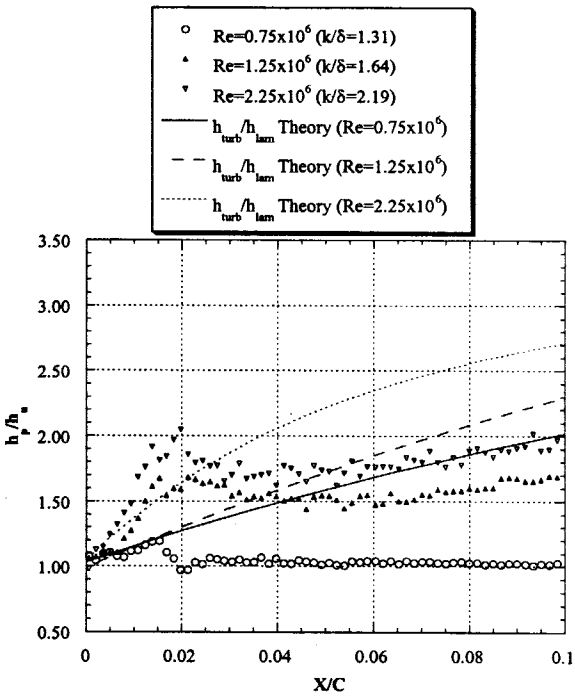

Fig. 8: Heat-transfer ratio profiles with 0.35mm roughness at 0.1% tunnel turbulence. Roughness between x/c=0.005 and 0.0138.

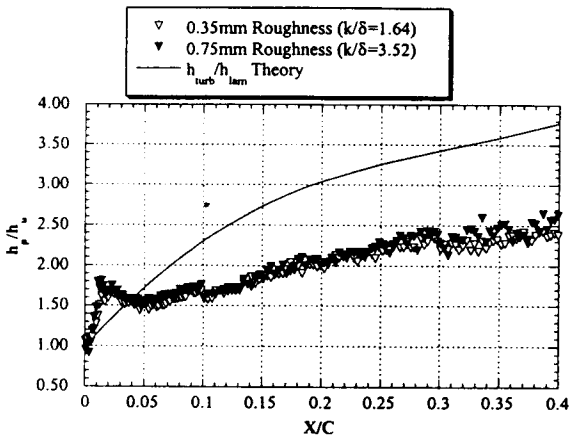

Fig. 9: Heat-transfer ratio profiles at 0.1% tunnel turbulence with 0.35mm and 0.75mm roughness. Roughness between x/c=0.005 and 0.0138. (Re=1.25x10^6)

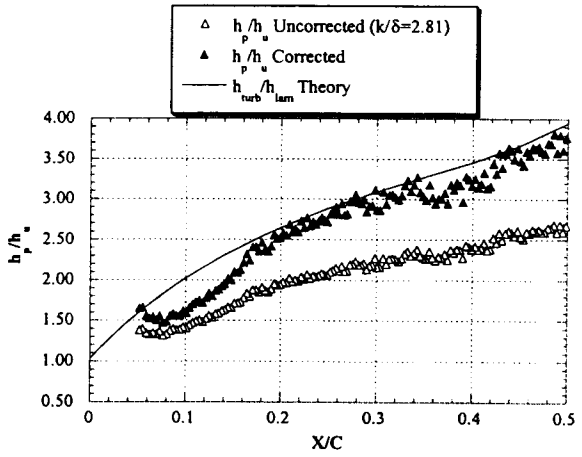

Fig. 11: Comparison of corrected and uncorrected heat-transfer ratio profiles with 0.75mm roughness at 0.1% tunnel turbulence. The corrected profile has (T_s-T_{aw}) profiles shifted down by 2.2 °F. Roughness between x/c=0.005 and x/c=0.0138. (Re=0.75x10^6)

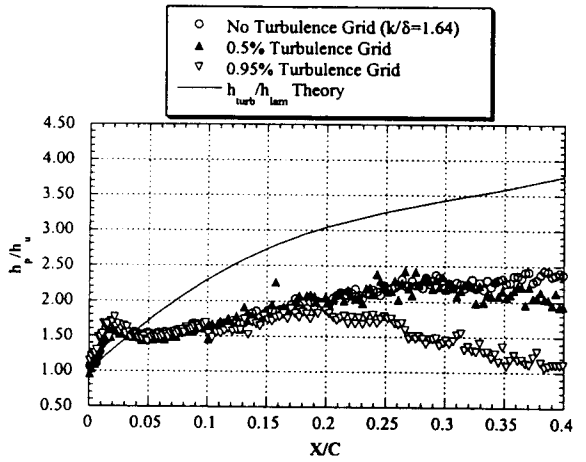

Fig. 10: Heat-transfer ratio profiles with 0.35mm roughness and varying tunnel turbulence levels. Roughness between x/c=0.005 and 0.0138. (Re=1.25x10^6)

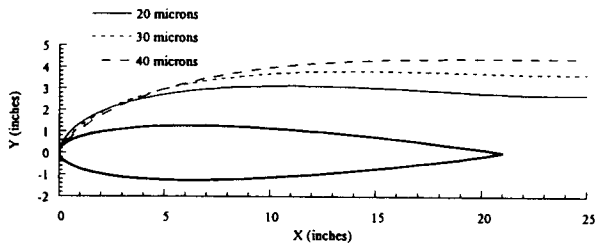

Fig. 12: Predicted droplet trajectories over a NACA 0012 airfoil at 8° angle of attack for three different drop sizes. Velocity 100 mph.

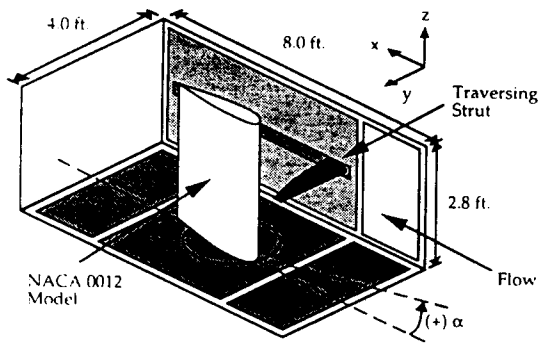

Fig. 13: Experimental setup of UIUC low-speed tunnel.

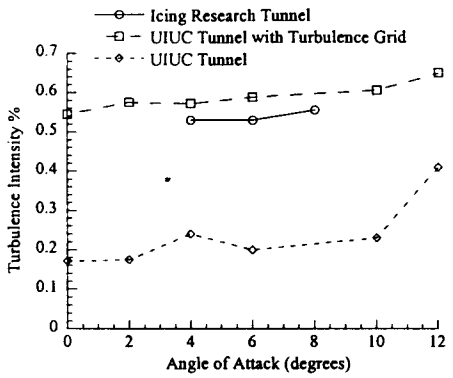

Fig. 14: Variation with angle of attack of turbulence intensity levels measured above a NACA 0012 airfoil. Approximate velocity 100 mph.

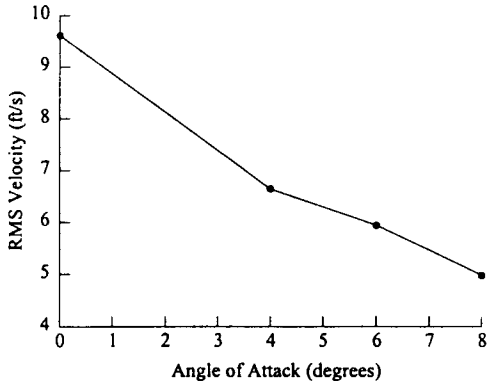

Fig. 17: RMS fluctuation of velocity signal including spikes due to droplet impingement as a function of angle of attack. LWC = 1.5g/m^3, MVD = 30 μm, U = 100 mph.

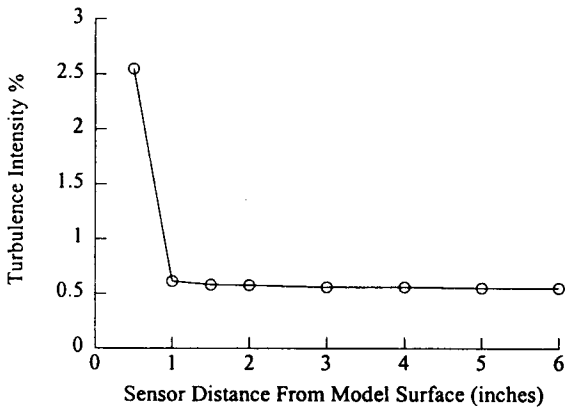

Fig 15: Turbulence intensity versus distance from model surface at approximately 85% chord. Data taken in UIUC tunnel at approximately 100 mph with turbulence grid installed.

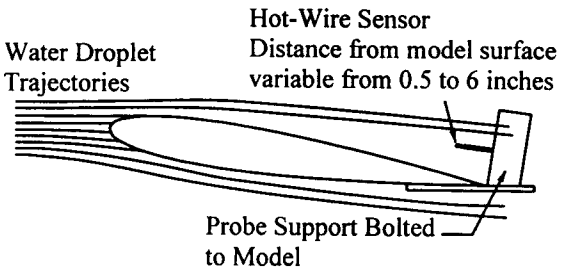

Fig. 16: Hot-wire probe mounted behind airfoil in the Icing Research Tunnel.

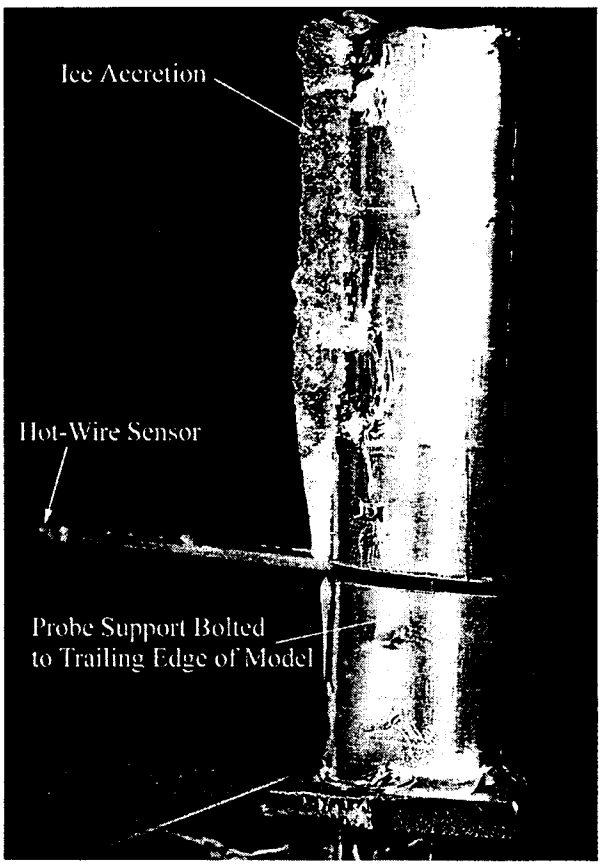

Fig. 18: Ice accretion on hot-wire mounting support. Model at 8 degrees angle of attack, U = 100 mph, T_{total} = 25 °F, MVD = 20 μm, LWC = 0.7g/m^3. (Photo courtesy of Dave Anderson, NASA Lewis Research Center)

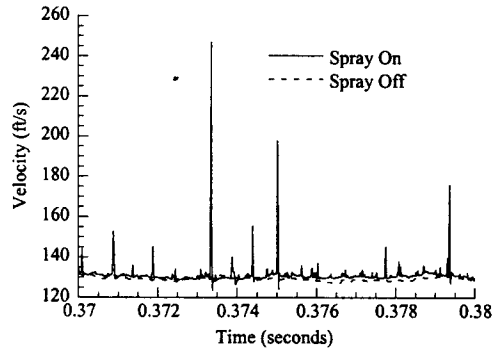

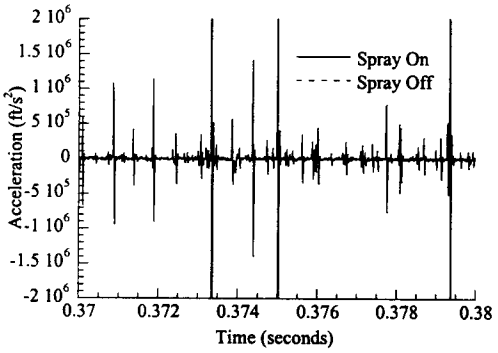

Fig. 19: 0.01 second velocity and acceleration time traces. Tunnel velocity = 100mph, model angle of attack = 8°, LWC = 1.5g/cm^3, MVD = 30 μm, sensor 1.5 inches from model surface.

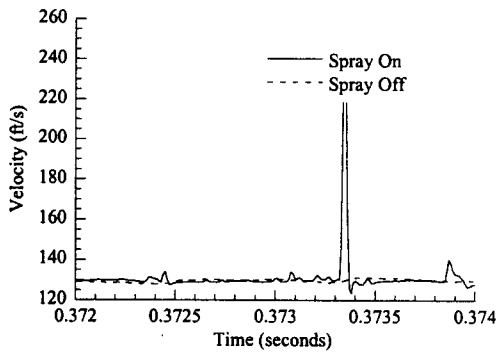

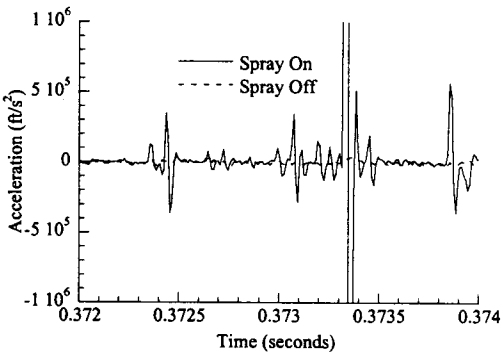

Fig. 20: 0.002 second velocity and acceleration time traces. Same data as Fig. 19.

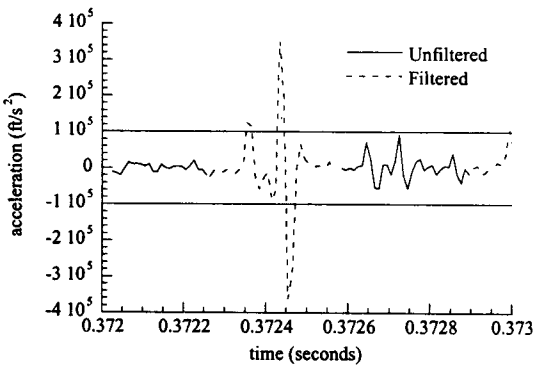

Fig. 21: Acceleration threshold filter. Horizontal lines represent threshold level. Dotted lines indicate data considered to be part of a droplet strike. Same data as shown in Figs. 19 and 20.

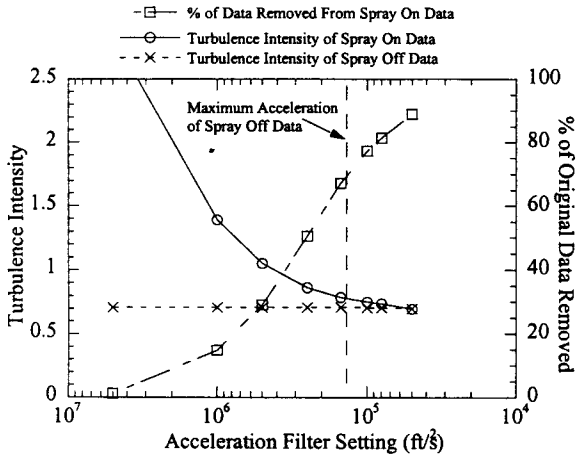

Fig. 22: Turbulence intensity and percent of data removed as a function of acceleration threshold setting. Turbulence intensity and maximum acceleration of corresponding spray off data are plotted for reference. Same data as in Figs. 19-21.

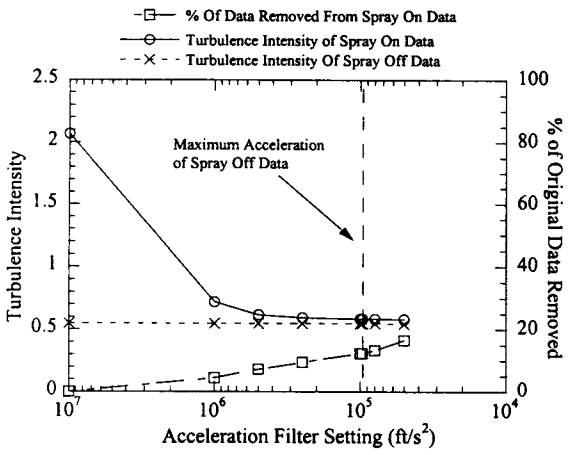

Fig. 23: Turbulence intensity and percent of data removed as a function of acceleration threshold setting. Turbulence intensity and maximum acceleration of corresponding spray off data are plotted for reference. Same conditions as Fig. 22 with LWC reduced to 0.9g/m³.

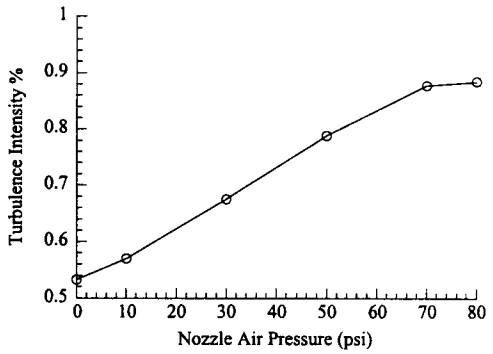

Fig. 24: Turbulence intensity variation with nozzle air pressure at 100 mph. Spray off.

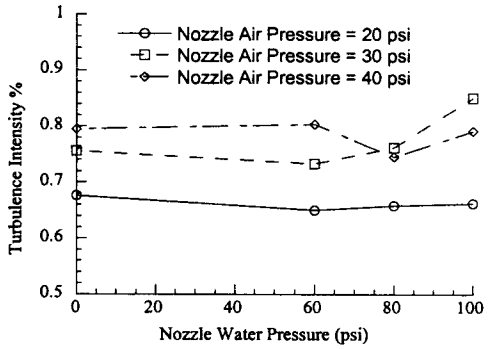

Fig. 25: Turbulence intensity as a function of spray nozzle water pressure at 3 spray nozzle air pressures.

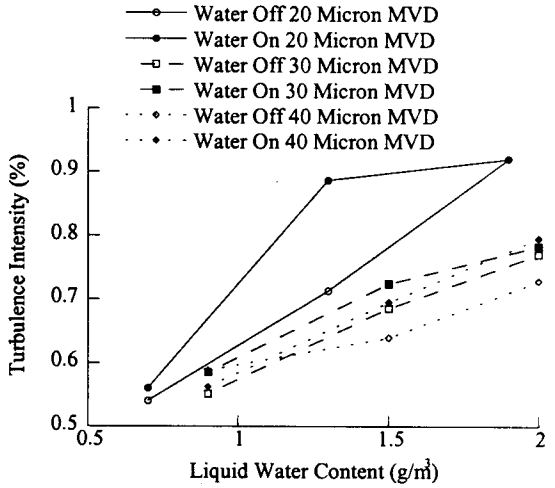

Fig. 26: Turbulence intensity versus LWC at three droplet sizes. Filtered spray on and corresponding spray off cases plotted for comparison.